Article

Solid-State Synthesis of SiC Particle-Reinforced AZ91D Composites: Microstructure and Reinforcement Mechanisms

Qian Shi [1,2], Pengxing Cui [2,3], Maoliang Hu [1,*], Fei Wang [1], Hongyu Xu [1] and Xiaobing Zhou [2,3,*]

1   School of Materials Science and Chemical Engineering, Harbin University of Science and Technology, Harbin 150080, China; shiqian@nimte.ac.cn (Q.S.); wfambitious@126.com (F.W.); xuhongyu@hrbust.edu.cn (H.X.)
2   Zhejiang Key Laboratory of Data-Driven High-Safety Energy Materials and Applications, Ningbo Institute of Materials Technology and Engineering, Chinese Academy of Sciences, Ningbo 315201, China; cuipengxing@nimte.ac.cn
3   Ningbo Key Laboratory of Special Energy Materials and Chemistry, Ningbo Institute of Materials Technology and Engineering, Chinese Academy of Sciences, Ningbo 315201, China
*   Correspondence: humaoliang@hrbust.edu.cn (M.H.); zhouxb@nimte.ac.cn (X.Z.); Tel.: +86-188-4641-0119 (M.H.); +86-135-8683-3856 (X.Z.)

Abstract: Safe and efficient recycling of industrially generated machined chips is a high-priority technological issue. In this study, the effect of SiC particles (SiCp) on the microstructure and mechanical properties of SiCp/AZ91D composites is systematically analyzed, and the reinforcement mechanism of SiCp on composites is investigated. Different contents of SiCp/AZ91D composites are fabricated by solid-state synthesis. The results show that the incorporation of SiCp refined the grains of SiCp/AZ91D composites, which is related to the uniform distribution of SiCp at the grain boundaries. The strong bonding of SiCp with the AZ91D matrix inhibited the generation and extension of cracks, which led to the simultaneous increase in the yield strength (YS) and elongation (EL) of the SiCp/AZ91D composites. The mechanical properties of the 3 wt.% SiCp/AZ91D composites are the most superior, with an average grain size, Vickers hardness, ultimate tensile strength (UTS), YS, and EL of 6.69 ± 4.48 μm, 89.5 ± 2.5 HV, 341 ± 11 MPa, 172 ± 8 MPa, and $4.43 \pm 0.18\%$, respectively. The reinforcement mechanisms of SiCp/AZ91D composites are mainly grain refinement and dislocation strengthening. Solid-state synthesis is an effective method for recycling magnesium alloy chips.

Keywords: AZ91D chips; recycling; solid-state synthesis; microstructure; reinforcement mechanisms

1. Introduction

Magnesium alloys offer significant advantages over aluminum alloys due to their light weight [1–6], high specific strength [7–9], and easy recovery [10,11], making them increasingly popular in fields such as automotive parts and electronic devices [12–16]. Due to their good machinability, the demand for magnesium alloys is increasing, resulting in a large amount of machining chips. The recycling of magnesium alloy processing chips is the key link to realize the sustainable use of resources and environmental protection, and it is also a problem that needs to be solved at present. Remelting is a common treatment method for these chips [17]. Asgari et al. [18] recycled and cleaned AZ91 alloy chips and fabricated SiC particle-reinforced magnesium matrix composites by melting and stirring using the stir casting method, realizing the sustainable use of waste magnesium chips. However, magnesium alloys are highly reactive and flammable [19], posing challenges to the remelting process. During remelting, magnesium alloys are prone to react with oxygen, moisture, and impurities to generate slag [20], which reduces melting efficiency and affects alloy properties. Its refining and casting require strict degassing, slag removal, and temperature control, which increase the production cost and technical difficulty, and require high equipment precision and operation technology [21]. Compared with the

traditional remelting process, solid-state synthesis technology has obvious advantages, as it can reduce the high-temperature exposure time, reduce oxidative burnout, reduce material and energy consumption, lower the cost [22], and provide a new method for the green and efficient recycling and reuse of magnesium alloys. Hu et al. [23] successfully realized the recycling of AZ31 alloy chips by the solid-state synthesis method. This method directly utilizes recycled magnesium alloy chips as raw materials, through cold or hot pressing the chips into billets by solid-state synthesis and then through hot extrusion molding at lower temperatures [24,25], which promotes elemental diffusion and obtains recycled magnesium alloy profiles with stable properties.

The AZ91D alloy is currently the most widely used cast magnesium alloy [26]; it has a finite slip system with a hexagonal closed-packed (HCP) structure [27–29], which leads to poor formability [30] and low strength [31,32]. When evaluating the feasibility of solid-state recycling of AZ91D alloy chips, the key engineering consideration is to ensure that the recycled material has excellent mechanical properties after extrusion. Wang et al. [33] found that the addition of hard ceramic particles to the AZ91D matrix improves its properties and thus better adapts it to various usage environments. Ceramic particles such as SiC, Al_2O_3, B_4C, and TiC are commonly used reinforcing phases for magnesium matrix composites [34,35], while SiC particles (SiCp) can be stabilized in AZ91D alloy due to their stable physical and chemical properties. Rauber et al. [36] found that the addition of SiCp increased the yield strength and ultimate tensile strength of AZ91D matrix composites by 21.43% and 6.91%, respectively, compared to AZ91D alloys. However, due to the small size effect [37], SiC nanoparticles usually form clusters, which limit the improvement of mechanical properties, and thus it is difficult to fabricate SiC-nanoparticle-reinforced metal matrix composites with high volume fractions. Pu et al. [38] discovered that the ultimate tensile and yield strengths of 15 vol.% 50 nm SiCp/7075Al composites were reduced by 5.91% and 9.66%, respectively, in comparison to 1.0 vol.% 50 nm SiCp/7075Al composites. Wang et al. [39] showed that 10 μm SiCp was uniformly distributed in the AZ91D matrix and significantly refined the grain size. The yield strength and ultimate tensile strength of 15 vol.% SiCp/AZ91D composites were increased by 21.43% and 6.91%, respectively, compared to 5 vol.% SiCp/AZ91D composites. Therefore, it is of great engineering significance to explore the effect of micro-SiCp on the microstructure and mechanical properties of AZ91D matrix composites.

At present, there are few articles on the solid-state recycling of AZ91 chips, especially on the microstructure and reinforcement mechanism of solid-state synthesized SiCp/AZ91 chip composites. In this study, different contents of micro-SiCp/AZ91D composites were prepared by solid-state synthesis using recycled AZ91D chips as the matrix and commercial SiCp as the reinforcing phase. The feasibility of solid-state recycling of AZ91D alloy chips was evaluated by systematically analyzing the microstructure and mechanical properties of SiCp/AZ91D composites.

2. Materials and Methods

2.1. Materials

The matrix material in this work was recycled AZ91D alloy chips (Northeast Light Alloy Co., Ltd., Harbin, China) with dimensions of (2 ± 0.5) mm $\times$ (1 ± 0.1) mm $\times$ (0.02 ± 0.001) mm. The chemical compositions (wt.%) of the AZ91D alloy chips were as follows: Al-9.3, Zn-0.7, Mn-0.23, Si-0.02, Cu-0.001, Ni-0.001, Fe-0.002, Be-0.0015, and Mg-balance. The reinforcement material was commercial SiCp (Shanghai Xinding metallurgical Co., Ltd., Shanghai, China).

2.2. Composites' Fabrication

The process parameters for the fabrication of SiCp/AZ91D composites are shown in Table 1. Micro-SiCp/AZ91D composites with different contents, denoted as AZ91D (0 wt.%), M-1 (1 wt.%), M-2 (2 wt.%), M-3 (3 wt.%), and M-4 (4 wt.%), were fabricated by solid-state synthesis. The fabrication process of AZ91D alloy from pure chips was consistent

with SiCp/AZ91D composites. First, mechanical milling was carried out using QM-3SP4-type planetary ball mills. The weight ratio of milling balls (ZrO$_2$, F 3 mm) to mixture (including AZ91 chips and SiCp) was 5:1 [40]. The g milling balls and mixture were loaded into a stainless steel ball milling jar and milled under vacuum for 2 h at 200 rpm [38,39]. Second, the mixture was cold-pressed to a cylindrical billet with Ø 40 mm × 40 mm by Y032-315 hydraulic press (Nantong Forging Equipment Rugao Co., Ltd., Rugao, China) at room temperature under a pressure of 600 MPa for 15 s [24]. Third, the billet was preheated at 410 °C for 30 min under a purified CO$_2$ atmosphere and directly extruded under a pressure of 650 MPa with an extrusion ratio of 25:1 and a speed of 0.2 mm/s [9,41]. Finally, the cylindrical rods with Ø 8 mm were obtained [24].

Table 1. The process parameters for the fabrication of SiCp/AZ91D composites.

Samples	SiCp Contents (wt.%)	SiCp Contents (wt.%)	Cold Pressure (MPa)	Holding Time (s)	Hot Extrusion Pressure (MPa)	Heating Temperature (°C)	Holding Time (min)
AZ91D	0	100					
M-1	1	99					
M-2	2	98	600	15	650	410	30
M-3	3	97					
M-4	4	96					

### 2.3. Microstructure and Property Test

The particle size analysis was performed on commercial SiC particles using a physical adsorption meter (ASAP2460, Mack, Greensboro, NC, USA). The phase composition of the samples was identified using an X-ray diffractometer (XRD; X-Pert PRO, Philips, The Netherlands) equipped with Cu Kα radiation at a diffraction angle (2θ) ranging from 20° to 100° [42]. The microstructure of SiCp/AZ91D composites was observed by an optical microscope (OM; LCMS301, Leica, Wetzlar, Germany). The distribution of SiCp in the AZ91D matrix was observed using a scanning electron microscope (SEM; G300, Zeiss, Oberkochen, Germany) equipped with an energy-dispersive spectrometer (EDS). The samples after etching with etchant (20 mL ethanol (95%) + 1 mL glacial acetic acid + 2 mL distilled water + 1 g picric acid) were used for OM and SEM analysis [33,43]. The average grain size of all the samples was measured using the linear intercept method, and the grain size distribution was analyzed by Image-pro Plus. The microstructure and interface of SiCp/AZ91D composite samples were analyzed using transmission electron microscopy (TEM; JEM-2100, JEOL, Tokyo, Japan). The Vickers hardness of SiCp/AZ91D composites was detected by an electromechanical universal testing machine (E44.304, MTS Systems Co., Ltd., Shanghai, China). The load was 0.98 N, and the dwell time was 15 s. To ensure the accuracy of the Vickers hardness, each sample was measured 5 times. The tensile samples with a length of 14 mm and cross-sectional areas of 6 mm × 2 mm [44] were prepared from the extruded SiCp/AZ91D composites by cutting along the extrusion direction (ED) according to the Chinese GB/T228-2002 standard [45]. Room-temperature tensile tests were conducted on an E44.304 electromechanical universal testing machine at a velocity of 1 mm/min. In order to ensure the accuracy of the tensile data, each sample was tested three times and the average tensile data for each set of experiments were obtained under the same conditions [46].

3. Results and Discussion

3.1. Microstructure

Figure 1 shows the characterizations of AZ91D alloy chips and SiC particles. Figure 1a illustrates that the chip's sides have jagged edges and its front is comparatively smooth. As seen in Figure 1b, the chips' lamellar surface (back) significantly increases the SiC particles' attachment sites. The microscopic morphology of SiC reinforcements is characterized by

irregular particle shape, as illustrated in Figure 1c. As shown in Figure 1d, the average particle size of commercial SiCp is 15.41 ± 3.91 μm.
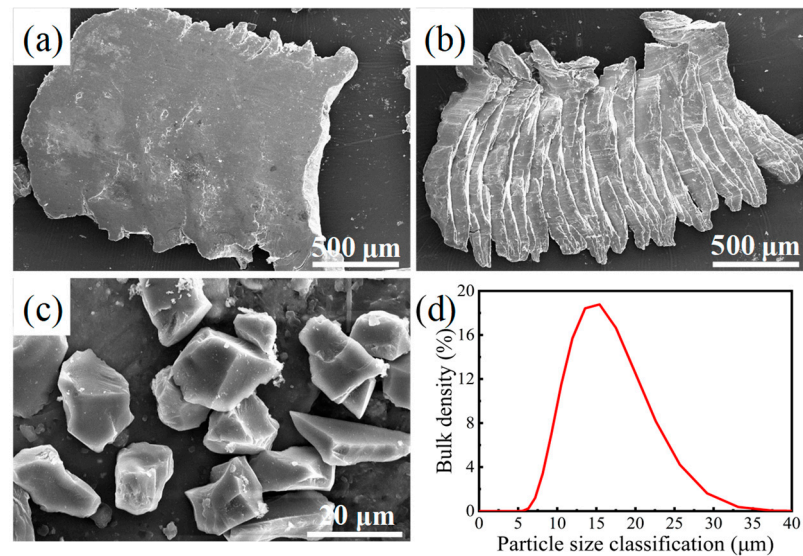
Figure 1. Characterizations of (**a**) AZ91D alloy chips (front); (**b**) AZ91D alloy chips (back); (**c**) the microscopic morphology of SiC particles; (**d**) the particle size distribution of SiC particles.

Figure 2 shows the XRD patterns of SiCp/AZ91D composites. The AZ91D alloy is composed mainly of α-Mg (JCPDS card No. 04-012-3405), with the β-$Mg_{17}Al_{12}$ (JCPDS card No. 04-010-7477) phase also present. These two phases were also identified in the SiCp/AZ91D composites. The particles are clearly identified as α-SiC (JCPDS card No. 04-012-5685) by the XRD results. The SiCp/AZ91D composites showed stronger α-SiC diffraction peaks, while weaker α-SiC diffraction peaks were not detected. The diffraction angle ranging from 33° to 39° is magnified for ease of distinction because the diffraction peaks of the α-SiC and β-$Mg_{17}Al_{12}$ phases are close to each other near 36°. Combined with the results of the JCPDS card, the diffraction peaks of SiC are observed at 34.1°, 35.7°, 38.1°, 60.0°, and 71.8°, corresponding to the (101), (006), (103), (110), and (116) planes, respectively. The XRD results show that the diffraction peak intensity of α-SiC in the SiCp/AZ91D composites increases with increasing SiCp content, which contributes to the grain refinement and the improvement in the mechanical properties of the SiCp/AZ91D composites.

Figure 3 shows the microstructure of the SiCp/AZ91D composite. Figure 3a indicates the sample's observation position parallel to the extrusion direction. SiCp are distributed on the grain boundaries, as shown in Figure 3b–f, and the SiCp are found at the grain boundaries with a "necklace" distribution [47,48]. During the hot extrusion process, the SiCp/AZ91D composites are subjected to three-dimensional compressive stress [49] (applied load: radial and axial), which resulted in a streamlined distribution of SiCp along the extrusion direction. This phenomenon has also been observed in previous studies by Cui et al. [50], Lv et al. [51], and Wang et al. [40]. As shown in Figure 3b, the average grain size of the AZ91D alloy is 12.69 ± 5.03 μm. As the SiCp content increased, the average grain size of the SiCp/AZ91D composites initially decreased and then increased. When the SiCp content was 3 wt.%, SiCp was uniformly distributed on the grain boundaries, and the average grain size of SiCp/AZ91D composites (6.69 ± 4.48 μm) decreased by 47.28% compared with that of AZ91D alloy, as shown in Figure 3e. However, at a SiCp content of 4 wt.%, the SiCp clusters were obvious, and the average grain size of the SiCp/AZ91D composites increased (9.18 ± 4.31 μm), as shown in Figure 3f. Doherty et al. [52] demonstrated that the particle deformation zone (PDZ) [23,53], which is a region of high dislocation density and large orientation gradient produced by forcing strain near non-deformed particles during the deformation process, is a perfect location for the nucleus of recrystallization to form. Therefore, SiCp facilitate the nucleation of dynamic recrystallization (DRX). The presence of

SiCp at grain boundaries also hinders the growth of grains in SiCp/AZ91D composites [54]. Solid-state synthesis refines the average grain size of SiCp/AZ91D composites for the two reasons mentioned above.
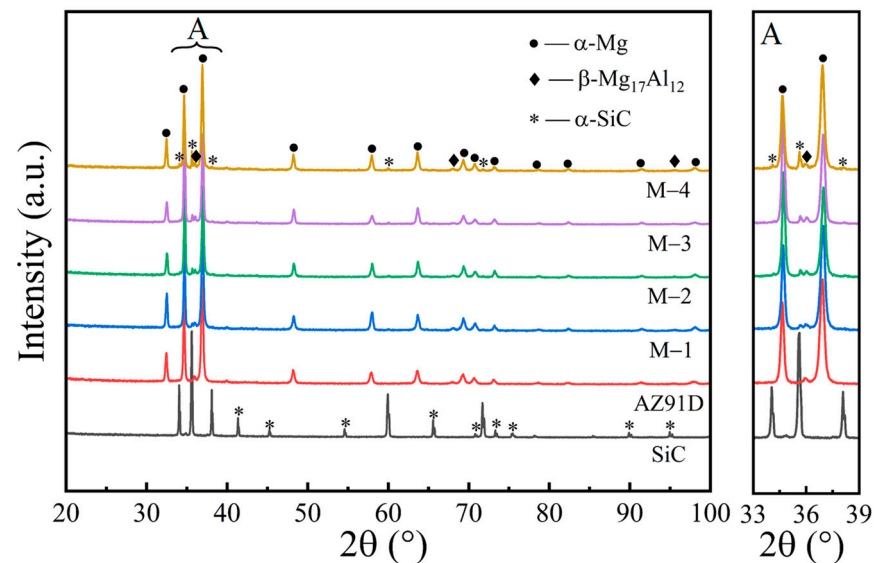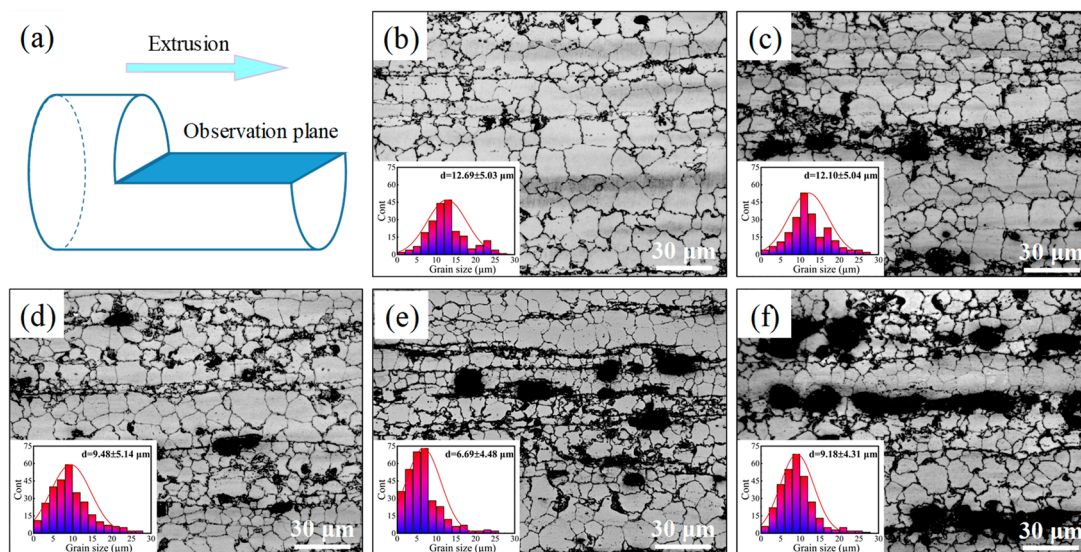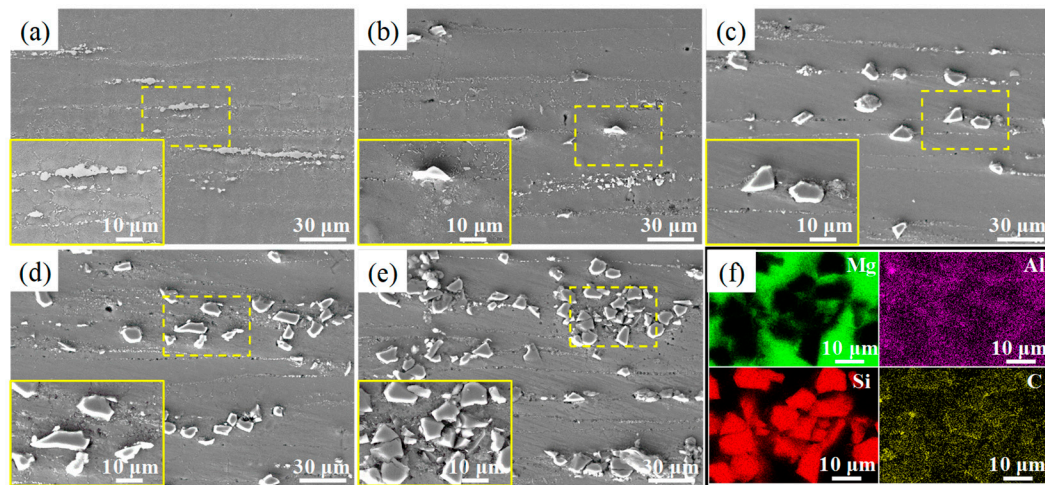

Figure 2. XRD patterns of SiCp/AZ91D composites.

Figure 3. OM microstructures of SiCp/AZ91D composites: (**a**) extrusion direction; (**b**) AZ91D; (**c**) M-1; (**d**) M-2; (**e**) M-3; (**f**) M-4. (The insets are the grain size distribution diagram).

Figure 4 shows the SEM microstructure and EDS results of the SiCp/AZ91D composites with different contents. In Figure 4a–e, the insets show SEM images of this material at high magnification in the yellow dashed box area. In Figure 4a, the β-Mg$_{17}$Al$_{12}$ phase is distributed on the grain boundaries along the extrusion flow line direction. As shown in Figure 4b–d, the reinforcements (gray irregular particles) of the 1, 2, and 3 wt.% SiCp/AZ91D composites are gradually increased and all of them show a homogeneous distribution on the grain boundaries. As the particle content continued to increase, larger particle clusters appeared in the 4 wt.% SiCp/AZ91D composite, as shown in Figure 4e. The EDS analysis shows that the gray particle clusters in Figure 4e are SiC particles. SiC particles are highly susceptible to agglomeration when their particle size is much smaller than the AZ91D chip size. In addition, in SiCp/AZ91D composites with higher mass

fractions, the smaller particle spacing results in particles that cannot flow easily during deformation. As a result, it is difficult for SiCp to be completely and uniformly dispersed in the SiCp/AZ91D composites that have been hot-extruded in one pass.

Figure 4. SEM microstructure and EDS results of SiCp/AZ91D composites (the inset is a partial enlargement): (**a**) AZ91D; (**b**) M-1; (**c**) M-2; (**d**) M-3; (**e**) M-4; (**f**) EDS results of (**e**).

In order to characterize the interfacial structure of SiCp with the Mg matrix, TEM micro-structure observation of 3 wt.% SiCp/AZ91D composites was carried out as shown in Figure 5. Figure 5a shows that SiCp is well bonded to α-Mg, while DRX grains and a large amount of dislocation buildup around SiCp are found. This finding was also reported in Shen et al. [47]. The difference in the coefficient of thermal expansion (CTE) between the AZ91D matrix (26×10^{-6} K^{-1}) and SiCp (4.8×10^{-6} K^{-1}) is high. During hot extrusion, dislocations build up around SiCp due to the strain mismatch between the SiCp and α-Mg [12,55]. On the one hand, dislocation stacking increases the critical shear stress required for dislocation motion, which in turn enhances the tensile strength of SiCp/AZ91D composites. On the other hand, with the incorporation of SiCp, the dislocation density and lattice distortion around the reinforcing particles increases, which promotes the nucleation of dynamically recrystallized grains [56]. Meanwhile, the uniform distributed SiCp in the SiCp/AZ91D composites hindered the migration of grain boundaries and inhibited the growth of re-crystallized grains, resulting in a refined grain size. Thus, the strength and Vickers hardness of the SiCp/AZ91D composites were further improved. Based on Figure 5b, a strong bond exists between SiCp and α-Mg, with a flat and smooth bonding surface that effectively prevents crack initiation and extension. The inverse Fourier transform (IFFT) of the region in the yellow dashed box in Figure 5c reveals significant dislocation accumulation in the matrix around the SiCp.
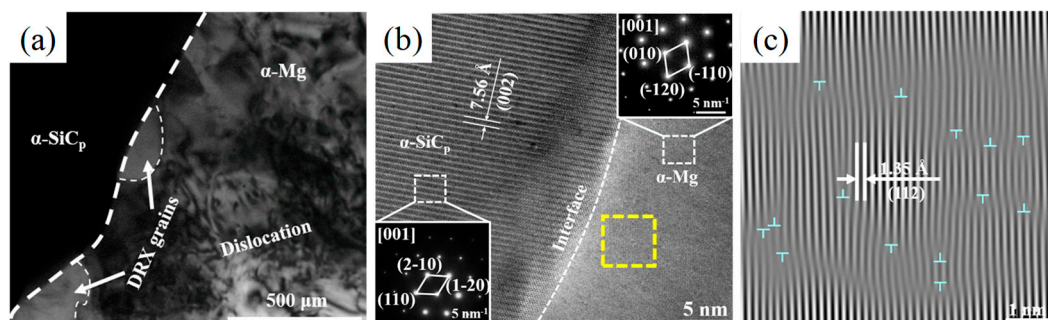
Figure 5. TEM microstructure of 3 wt.% SiCp/AZ91D composites: (**a**) TEM micrographs; (**b**) HRTEM (the insets are diffraction pattern of α-SiCp and α-Mg); (**c**) IFFT of α-Mg.

3.2. Mechanical Properties

Figure 6 shows the Vickers hardness of the SiCp/AZ91D composites. When the SiCp content is 1 wt.%, the Vickers hardness is 20.1% higher than that of the AZ91D alloy (70.0 ± 2.6 HV). It illustrates that the Vickers hardness of the SiCp/AZ91D composites is improved after adding SiCp. After that, with increasing SiCp content, the Vickers hardness of the SiCp/AZ91D composites also gradually increases. The main reasons for the increase in the Vickers hardness of the SiCp/AZ91D composites are as follows: (1) The addition of SiCp refines the AZ91D matrix grain, as shown in Figure 3. Finer grains mean more grain boundaries, which are effective barriers against the plastic deformation of the matrix. (2) As shown in Figure 4, the high-hardness SiCp are uniformly dispersed on the grain boundaries, which are able to withstand and transfer externally applied loads. This load transfer mechanism effectively prevents plastic deformation in the matrix. (3) Dislocation plugging exists at the interface between SiCp and the AZ91D matrix, as shown in Figure 5. These dislocations increase the strain-hardening capacity of the matrix, thereby increasing the hardness of the composite during plastic deformation. However, when the SiCp content is 4 wt.%, the Vickers hardness (89.7 ± 2.0 HV) of the SiCp/AZ91D composites is almost equal to that of 3 wt.% SiCp/AZ91D composites, and which is 28.1% higher than that of the AZ91D alloy. Morisada et al. [57] and Figures 3 and 4 demonstrate that clustered SiCp inhibit the refinement of matrix grains and reduce the deformation resistance of the matrix. This ultimately leads to a decrease in the Vickers hardness of the 4 wt.% SiCp/AZ91D composites.
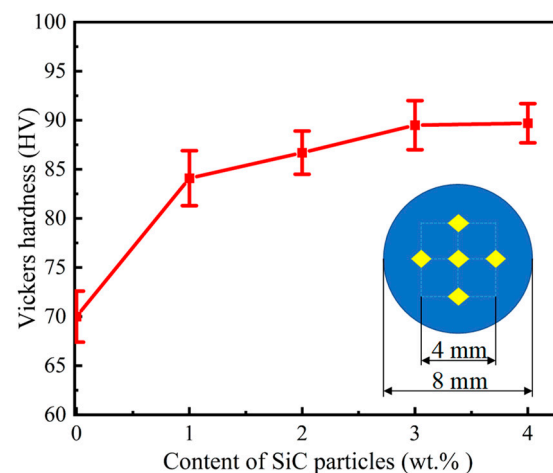

Figure 6. Vickers hardness of SiCp/AZ91D composites (the inset is an indentation diagram).

Figure 7 shows the engineering stress–strain curves and the mechanical properties of the SiCp/AZ91D composites. It is apparent that the SiCp/AZ91D composites exhibits higher strength. Figure 7a shows the stress–strain curves of the SiCp/AZ91D composites. It demonstrates that the stress increases and then decreases with increasing SiCp content. Specifically, as shown in Figure 7b, the yield strength (YS) and ultimate tensile strength (UTS) of the SiCp/AZ91D composites gradually increase and then decrease with the increase in SiCp content, and the elongation (EL) follows the same trend as the strength. The YS and UTS of the AZ91D alloy are 138 ± 10 MPa and 227 ± 11 MPa, respectively. After adding 3 wt.% SiCp, the YS and UTS are increased to 172 ± 8 MPa and 341 ± 11 MPa, respectively. The corresponding improvements in the YS and UTS are 24.64% and 50.22%, respectively, which illustrates that the tensile properties of the SiCp/AZ91D composites can be improved significantly by solid-state synthesis. However, when the SiCp content is 4 wt.%, the YS and UTS significantly decrease due to the presence of SiCp clusters in the AZ91D matrix, which is consistent with the OM observation in Figure 3e. As mentioned in Section 3.1, solid-state synthesis has a significant effect on refining the grain size and

improving the particle distribution. Uniform particle distribution and fine grain size significantly improved the strength of particle-reinforced metal matrix composites [58].
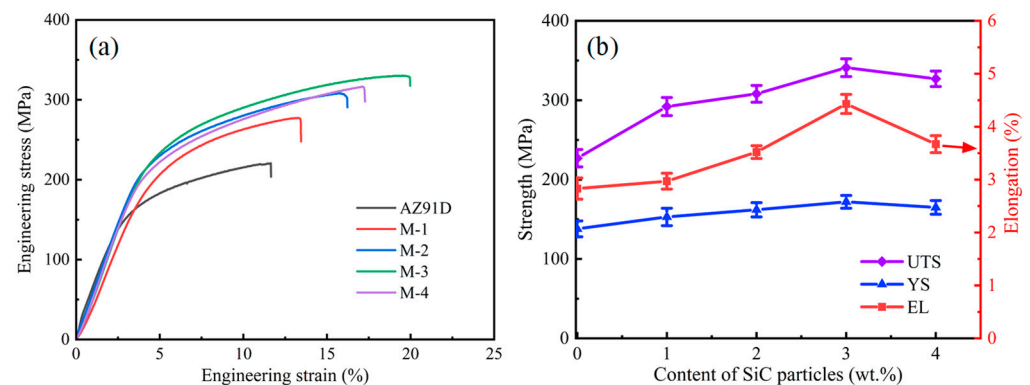
Figure 7. (**a**) Engineering stress–strain curves; (**b**) the mechanical properties of SiCp/AZ91D composites.

Figure 8 shows the tensile fracture morphology of the SiCp/AZ91D composites. AZ91D alloys are more susceptible to brittle fracture under tensile loading due to their densely arranged hexagonal (HCP) crystal structure, which results in a limited slip system [46,59]. The tensile fracture of the SiCp/AZ91D composite shown in Figure 8b–d,f is a disintegrated fracture with more dimples (purple arrows) [60], tearing ridges (green arrows) [61], cleavage planes (red arrows) [62], and cracks (yellow curves) [63] on the fracture. The fracture of AZ91D is dominated by tearing ridges and long bending cracks as shown in Figure 8a, and this fracture is considered brittle [64]. As shown in Figure 8b–d, with the increase in SiCp content, the number of long bending cracks at the fracture of the SiCp/AZ91D composites decreases, short cracks appear, and toughness is enhanced. This is consistent with the tensile test results of the SiCp/AZ91D composites, as the incorporation of SiCp refines the matrix grain size, which is consistent with the results observed in Figure 3. The reduction in grain size and increase in grain boundaries lead to crack deflection and crack tip passivation during extension, which improve the toughness of SiCp/AZ91D composites [65]. The increased toughness nests and decreased tear prongs indicate that the fracture mechanism of the 1, 2, and 3 wt.% SiCp/AZ91D composites is predominantly toughness [66]. In other studies, the fracture surfaces of SiC/AZ91 composites have shown that cracks around the ceramic particles lead to a de-bonding of the particles from the matrix and the fracture of the composite [67,68]. As shown in Figure 8d,e, in this study, the SiCp found inside the tough fossa of 3 wt.% SiCp/AZ91D composites showed less interfacial de-bonding and micro-cracking during fracture. Typically, the presence of a large number of particles leads to higher stress concentrations because of the higher dislocation density surrounding them [69,70]. This is consistent with the observation in Figure 5a. As the SiCp content increased to 4 wt.%, a large number of cracks appeared at the fracture of the SiCp/AZ91D composite, as shown in Figure 8f. The number of long bending cracks and the crack width around the SiCp clusters increased significantly, the plasticity of the 4 wt.% SiCp/AZ91D composites decreased, and the fracture type became brittle fracture [59]. This is consistent with the tensile test results of the 4 wt.% SiCp/AZ91D composites.
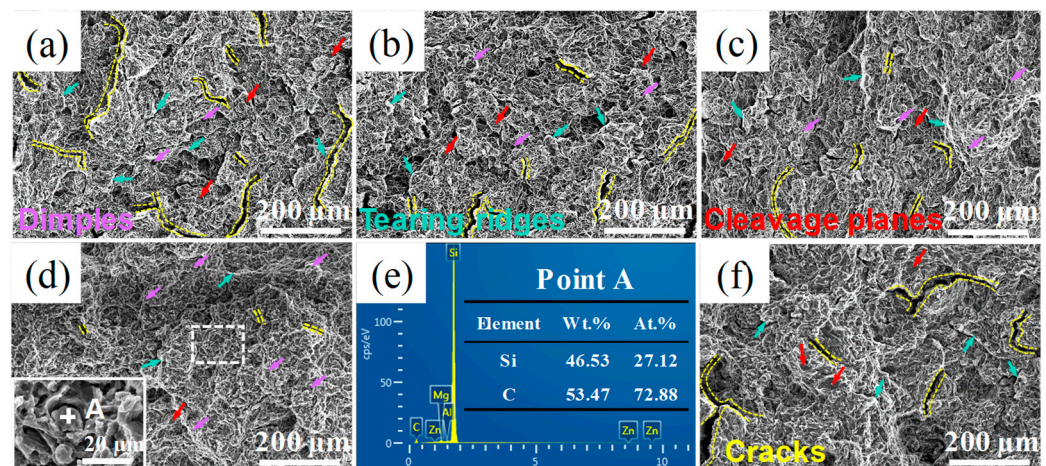
Figure 8. Fracture morphology of SiCp/AZ91D composites: (**a**) AZ91D; (**b**) M-1; (**c**) M-2; (**d**) M-3 (the inset is a partial enlargement); (**e**) EDS mapping results at point A; (**f**) M-4.

The addition of SiCp improves the strength and hardness of the matrix material, which makes it difficult for SiCp/AZ91D composites to undergo plastic deformation and fracture. At the same time, the fine and uniformly distributed SiCp play a role in dispersing the stress and reducing the stress concentration, thus delaying the crack generation and extension [71]. At low SiCp content, the fracture of SiCp/AZ91D composites mainly occurs in the matrix. The fracture mechanism of SiCp/AZ91D composites is still dominated by brittle fracture due to the poor toughness of magnesium alloys, which have HCP structures [46]. However, when the reinforcing phase content is too high, the continuity of the matrix is disrupted. The fracture mechanisms of the composite are brittle fracture and interfacial segregation, which reduce the mechanical properties of the composite. Wang et al. [72] demonstrated that the main mode of crack formation in particle-dense zones is interfacial segregation, which is attributed to the formation of weak interfaces in the composites and the formation of a large concentration of stresses in the agglomerated SiCp. The interface of a composite is the "bridge" between the metal matrix and the reinforcement. In tensile tests, the load is transferred from the metal matrix to the reinforcement through the interface [12]. When the interfacial bond is weak, cracks are easily generated and extended at the interface, whereas when the interfacial bond is strong, fracture occurs within the particles or in the matrix.

3.3. Reinforcement Mechanisms

To sum up, the reinforcement mechanisms are the grain refinement strengthening mechanism, the load transfer mechanism, and the dislocation strengthening mechanism. The reinforcement mechanisms are analyzed as follows.

The relational expression of YS change caused by load transfer in particle-reinforced composites is as follows [27,73]:

$$\Delta\sigma_{\text{Load}} = 0.5V_{\text{p}}\sigma_{\text{M}} \tag{1}$$

where $\Delta\sigma_{\text{Load}}$ is the YS of the SiCp/AZ91D composites. σ_{M} is the YS of the AZ91D matrix. V_{p} is the volume fraction of SiCp in the composites.

A theoretical model of the influence of fine grain strengthening on YS can be expressed by the Hall–Petch formula, which is estimated by the following equation [6]:

$$\Delta\sigma_{\text{Hall-Petch}} = K\left(D_{\text{composites}}^{-1/2} - D_{\text{AZ91}}^{-1/2}\right) \tag{2}$$

where $\Delta\sigma_{\text{Hall-Petch}}$ is the YS of the SiCp/AZ91D composites. K is the constant (0.10 MPa/m). $D_{\text{composites}}$ is the average grain size of the SiCp/AZ91D composites. D_{AZ91D} is the average grain size of the AZ91D matrix.

The relational expression of YS change caused by dislocation strengthening is as follows [74]:

$$\Delta\sigma_{\text{CTE}} = \alpha G b \sqrt{\frac{12\Delta\alpha\Delta TV}{bD(1-V)}} \tag{3}$$

where $\Delta\sigma_{\text{CTE}}$ is the increased YS of the SiCp/AZ91D composites. α is the dislocation strengthening coefficient. G is the shear modulus of the AZ91D matrix (16.60 GPa). b is the Burgers vector (0.32 nm). $\Delta\alpha$ is the difference in the thermal expansion coefficient between SiCp and the AZ91D matrix (21.2×10^{-6} K^{-1}). D is the SiCp diameter.

Based on Equations (1)–(3), the theoretical increments of YS for the SiCp/AZ91D composites were calculated as shown in Figure 9. The $\Delta\sigma_{\text{Load}}$ and $\Delta\sigma_{\text{CTE}}$ of the SiCp/AZ91D composites both increase with the increase in SiCp content, where the dislocation strengthening effect is more pronounced. The $\Delta\sigma_{\text{Hall-Petch}}$ value of the 3 wt.% SiCp/AZ91D composites is the highest, which indicates that $\Delta\sigma_{\text{Hall-Petch}}$ does not increase with the increase in SiCp content. The highest value of $\Delta\sigma_{\text{Hall-Petch}}$ shows that $\Delta\sigma_{\text{Hall-Petch}}$ does not increase with the increase in SiCp content. The effect of fine grain strengthening is directly related to the grain size, which is closely related to the dispersion of SiCp. SiCp/AZ91D composites are anticipated to have finer grain sizes and superior mechanical properties due to the high volume fraction of SiCp added to the alloy and the uniform dispersion of SiCp throughout the matrix.
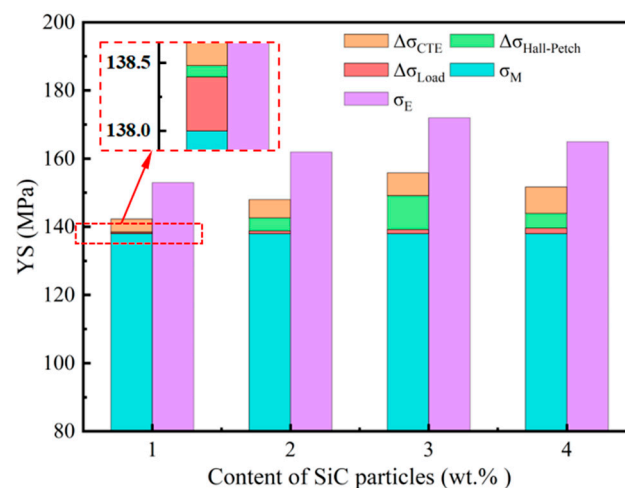
Figure 9. Contribution of strengthening mechanism to YS of SiCp/AZ91D composites.

Based on the above microstructural observation and assessment, a schematic illustration of the AZ91D matrix's microstructure influenced by SiCp during solid-state synthesis was established, as shown in Figure 10. Grain size and second-phase distribution can significantly affect the mechanical properties of magnesium alloys. Regarding the effect of grain size on the mechanical properties of magnesium alloys, it was reported that the new phase is easily nucleated at the grain boundaries due to the large dislocation at the grain boundaries, high grain boundary energy, and large atomic activity in the process of solid-state phase transformation. Moreover, the atomic arrangement at the grain boundaries is irregular, and the existence of grain boundaries at room temperature will impede the movement of dislocations, resulting in increased resistance to plastic deformation. Therefore, the finer the grain size and the more grain boundaries there are, the higher the nucleation rate of the new phase and the greater the strength of the material. The second phase can also play an important role in the mechanical properties of magnesium alloys [75]: parameters such as volume fraction, size, and distribution can modify the role of the second phase, even if they exhibit excellent physical properties. Deng et al. [67] reported that the addition of 0.2 vol.% submicron SiCp could refine the grain size of the AZ91D matrix and improve the YS and

UTS of SiCp/AZ91D composites, and further increasing the content of SiCp to 0.5 vol.% increased the grain size and decreased the YS and UTS of SiCp/AZ91D composites.
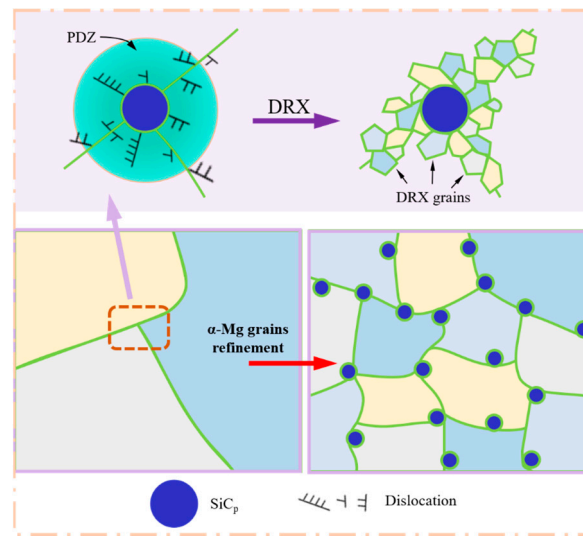
Figure 10. The schematic illustration of AZ91D matrix's microstructure influenced by SiCp.

In the vicinity of the second-phase particles (SiCp) and grain boundaries, stress concentration often occurs due to thermal and tissue stresses, and dislocations are generated in this region when the stress is high enough to cause slippage in the local area. During the extrusion process, due to the uncoordinated deformation between SiCp and the substrate, a PDZ can easily form around SiCp [76]. This region has a high dislocation density and deformation degree, which is conducive to the recrystallization and nucleation of the matrix grains. With the increase in SiCp content, during the plastic deformation process, the number of dislocations in the crystal will continue to increase. The presence of a large number of dislocations during the slip surface movement process, such as encountering obstacles (fixed dislocations, SiCp, grain boundaries, etc.), leads to dislocations in front of the obstacles being stopped and the subsequent dislocations being blocked up; the result is the formation of dislocation plugging. A high-density dislocation zone is conducive to promoting recrystallization nucleation, so that the grain can be refined. When SiCp are densely distributed on the grain boundaries, i.e., there are SiCp clusters at the grain boundaries, where a high degree of stress concentration is generated due to the obstruction of dislocation movement, this weakens the bonding of the grain boundaries and causes interfacial separation during the tensile process.

4. Conclusions

In this study, SiCp/AZ91D composites with excellent mechanical properties are successfully prepared by solid-state synthesis using recycled AZ91D chips as the matrix, confirming the possibility of solid-state recycling of magnesium alloy chips. In this study, the effects of SiCp on the microstructure and mechanical properties of the composites are systematically analyzed, the reinforcement mechanism of SiCp on the composites is investigated, and the following conclusions are drawn.

(1) AZ91D chips are recycled directly into new magnesium products without pretreatment. The SiCp particles are uniformly dispersed in the SiCp/AZ91D composites through the ball milling process. After hot extrusion, the SiCp are well bonded to the magnesium matrix. Solid-state recovery of magnesium alloy chips is confirmed to be an advanced technology that effectively utilizes waste chips, reduces costs, and achieves resource recycling.

(2) SiCp are able to refine the microstructure of magnesium alloy. When the SiCp content is 3 wt.%, the average grain size of the SiCp/AZ91D composites is the most refined, and the average grain size is reduced from 12.69 ± 5.03 um to 6.69 ± 4.48 μm.

(3) With the increase in SiCp content, the mechanical properties of the SiCp/AZ91D composites show a trend of increasing and then decreasing. When the content of SiCp is 3 wt.%, the mechanical properties of the SiCp/AZ91D composites are excellent, with Vickers hardness, YS, UTS, and EL of 89.5 ± 2.5 HV, 172 ± 8 MPa, 341 ± 11 MPa, and 4.43 ± 0.18%, respectively. The strong bonding of SiCp with the AZ91D matrix inhibited crack initiation and extension. The fracture mode of the SiCp/AZ91D composites is brittle cleavage fracture.

(4) SiCp improve the strength–toughness of the AZ91D matrix by hindering grain boundary migration, increasing dislocation density, and promoting dynamic recrystallization nucleation. The strengthening mechanisms of the SiCp/AZ91D composites are mainly the grain refinement strengthening mechanism and the dislocation reinforcement mechanism, and the load transfer mechanism has little effect on the mechanical properties.

References

1. Xie, Q.M.; Wu, Y.X.; Wu, Y.Z.; Peng, S.L. Study on the Optimization of Heat Transfer Coefficient of a Rare Earth Wrought Magnesium Alloy in Residual Stress Analysis. *Metals* **2024**, *14*, 222. [CrossRef]

2. Liang, M.J.; Zheng, J.; Liu, H.; Yao, B.X. Microstructure and mechanical properties of AZ31 alloy prepared by cyclic expansion extrusion with asymmetrical extrusion cavity. *Trans. Nonferrous Met. Soc. China* **2022**, *32*, 122–133. [CrossRef]

3. Geng, K.J.; Jiang, H.P.; Zhang, S.Q.; Gao, X.; Wu, J.H.; Sun, C.C.; Zhou, J.X.; Zhang, X.F. Effects of Mold Temperature on the Microstructures and Tensile Properties of the Thixoforged Graphite/AZ91D Composite. *Metals* **2023**, *13*, 1000. [CrossRef]

4. Sarvesha, R.; Chalapathi, D.; Yadava, M.; Jain, J.; Singh, S.S. In-situ studies on deformation and fracture characteristics of AZ91 Mg alloy. *Materialia* **2021**, *18*, 101177. [CrossRef]

5. Farzami, M.; Farahani, M.; Akbari, D.; Tabasi, M. Friction Stir Weld of AZ91 Magnesium Alloy With and Without Nano-SiC Particle. *JOM* **2019**, *71*, 4171–4179. [CrossRef]

6. Lee, T.; Yamasaki, M.; Kawamura, Y.; Go, J.B.; Park, S.H. High-Strength AZ91 Alloy Fabricated by Rapidly Solidified Flaky Powder Metallurgy and Hot Extrusion. *Met. Mater. Int.* **2019**, *25*, 372–380. [CrossRef]

7. Braga, P.L.; de Souza, D.C.P.; de Oliveira, M.C.L.; Antunes, R.A. Effect of Graphene Oxide as an Anodizing Additive for the ZK60A Magnesium Alloy: Correlating Corrosion Resistance, Surface Chemistry and Film Morphology. *Metals* **2024**, *14*, 210. [CrossRef]

8. Du, Z.Q.; Deng, K.K.; Nie, K.B.; Wang, C.J.; Xu, C.; Shi, Q.X. High-Modulus Laminated SiC/AZ91 Material with Adjustable Microstructure and Mechanical Properties Based on the Adjustment of the Densities of the Ceramic Layers. *Materials* **2023**, *16*, 6168. [CrossRef] [PubMed]

9. Liu, F.X.; Wang, Z.H.; Du, X.; Li, S.B.; Du, W.B. Microstructure and Mechanical Properties of Magnesium Matrix Composites Reinforced by In Situ Reduced Graphene Oxide. *Materials* **2023**, *16*, 2303. [CrossRef]

10. Zhou, X.J.; Zhang, Z.F.; Li, X.L.; Zhou, L.Y.; Zhang, X.D.; Chen, M.J. Microstructure and Phase Evolution Characteristics of the In Situ Synthesis of TiC-Reinforced AZ91D Magnesium Matrix Composites. *Materials* **2022**, *15*, 1278. [CrossRef]

11. Zhang, X.L.; Yu, G.K.; Zou, W.B.; Ji, Y.S.; Liu, Y.Z.; Cheng, J.L. Effect of casting methods on microstructure and mechanical properties of ZM5 space flight magnesium alloy. *China Foundry* **2018**, *15*, 418–421. [CrossRef]

12. Nie, K.B.; Wang, X.J.; Deng, K.K.; Hu, X.S.; Wu, K. Magnesium Matrix Composite Reinforced by Nanoparticles—A review. *J. Magnes. Alloy.* **2021**, *9*, 57–77. [CrossRef]

13. Hassana, S.F.; Tunb, K.S.; Guptab, M. Effect of Sintering Techniques on the Microstructure and Tensile Properties of Nano-Yttria Particulates Reinforced Magnesium Nanocomposites. *J. Alloys Compd.* **2011**, *509*, 4341–4347. [CrossRef]

14. Goh, C.S.; Wei, J.; Lee, L.C.; Gupta, M. Properties and deformation behaviour of Mg-Y_2O_3 nanocomposites. *Acta Mater.* **2007**, *55*, 5115–5121. [CrossRef]

15. Song, J.F.; She, J.; Chen, D.L.; Pan, F.S. Latest Research Advances on Magnesium and Magnesium Alloys Worldwide. *J. Magnes. Alloy.* **2020**, *8*, 1–41. [CrossRef]

16. Zhu, H.D.; Li, X.T.; Guan, X.R.; Shao, Z.C. Effect of Molybdate Conversion Coating of Magnesium Alloy Reinforced by Micro-arc Oxidation. *Met. Mater. Int.* **2021**, *27*, 3975–3982. [CrossRef]

17. Wang, J.Y.; Lin, Y.N.; Chang, T.C.; Lee, S. Recycling the Magnesium Alloy AZ91D in Solid State. *Mater. Trans.* **2006**, *47*, 1047–1051. [CrossRef]

18. Asgari, A.; Sedighi, M.; Krajnik, R. Magnesium alloy-silicon carbide composite fabrication using chips waste. *J. Clean. Prod.* **2019**, *232*, 1187–1194. [CrossRef]

19. Dudek, P.; Piwowońska, J.; Polczyk, T. Microstructure of castings made of magnesium alloys based on recycling of the circulating scrap. *J. Mater. Res. Technol.* **2021**, *14*, 2357–2364. [CrossRef]

20. Schramm, A.; Recksiek, V.; Dudczig, S.; Scharf, C.; Aneziris, C. Immersion Testing of Variously Coated Ceramic Foam Filters in an AZ91 Magnesium Melt. *Adv. Eng. Mater.* **2021**, *24*, 2100519. [CrossRef]

21. Schramm, A.; Nowak, R.; Bruzda, G.; Polkowski, W.; Fabrichnaya, O.; Aneziris, C.G. High temperature wettability and corrosion of ZrO_2, Al_2O_3, Al_2O_3-C, MgO and MgAlON ceramic substrates by an AZ91 magnesium alloy melt. *J. Eur. Ceram. Soc.* **2022**, *42*, 3023–3035. [CrossRef]

22. Wu, S.Y.; Ji, Z.S.; Hu, M.; Huang, Z.Q.; Tian, C.Y.; Wu, M.Z. Microstructure and Mechanical Properties of AZ31B Magnesium Alloy Prepared by Solid State Recycling. *Rare Met. Mater. Eng.* **2018**, *47*, 736–741. [CrossRef]

23. Hu, M.L.; Wei, S.H.; Shi, Q.; Ji, Z.S.; Xu, H.Y.; Wang, Y. Dynamic Recrystallization Behavior and Mechanical Properties of Bimodal Scale Al_2O_3 Reinforced AZ31 Composites by Soild State Synthesis. *J. Magnes. Alloy.* **2020**, *8*, 841–848. [CrossRef]

24. Wei, S.H.; Hu, M.L.; Ji, Z.S.; Xu, H.Y.; Wang, Y. Evaluation of microstructure and properties of AZ31/Al_2O_3 composites prepared by solid-phase synthesis. *Mater. Sci. Technol.* **2018**, *34*, 2097–2104. [CrossRef]

25. TesaŘ, K.; BalÍK, K.; Sucharda, Z.; JÄGer, A. Direct extrusion of thin Mg wires for biomedical applications. *Trans. Nonferrous Met. Soc. China* **2020**, *30*, 373–381. [CrossRef]

26. Zhao, C.; Ma, G.; Liu, T.; Hu, M.; Ji, Z. Effect of Near-Liquidus Squeeze Casting Pressure on Microstructure and Mechanical Property of AZ91D Alloy Differential Support. *Materials* **2023**, *16*, 4020. [CrossRef]

27. Huang, S.J.; Diwan Midyeen, S.; Subramani, M.; Chiang, C.C. Microstructure Evaluation, Quantitative Phase Analysis, Strengthening Mechanism and Influence of Hybrid Reinforcements (β-SiCp, Bi and Sb) on the Collective Mechanical Properties of the AZ91 Magnesium Matrix. *Metals* **2021**, *11*, 898. [CrossRef]

28. Liu, S.S.; Yang, B.P.; Huang, G.S.; Chen, X.H.; Tang, A.t.; Jiang, B.; Zheng, K.H.; Pan, F.S. Effect of dual-heterogeneous microstructures on mechanical properties of AZ91 extruded sheet. *Trans. Nonferrous Met. Soc. China* **2023**, *33*, 1086–1097. [CrossRef]

29. Hong, X.; Meng, L.; Yupeng, W.; Pinkui, M.; Ming, B.; Bo, J.; Zhipeng, G.; Yujie, Z. Refined microstructure and dispersed precipitates in a gradient rolled AZ91 alloy under pulsed current. *Materialia* **2021**, *20*, 101245. [CrossRef]

30. Liu, W.J.; Jiang, B.; Luo, S.Q.; Chen, S.Q.; Pan, F.S. Mechanical properties and failure behavior of AZ61 magnesium alloy at high temperatures. *J. Mater. Sci.* **2018**, *53*, 8536–8544. [CrossRef]

31. Deng, K.K.; Wang, X.J.; Wu, Y.W.; Hu, X.S.; Wu, K.; Gan, W.M. Effect of Particle Size on Microstructure and Mechanical Properties of SiCp/AZ91 Magnesium Matrix Composite. *Mater. Sci. Eng. A* **2012**, *543*, 158–163. [CrossRef]

32. Kandemir, S. Development of Graphene Nanoplatelet-Reinforced AZ91 Magnesium Alloy by Solidification Processing. *J. Mater. Eng. Perform.* **2018**, *27*, 3014–3023. [CrossRef]

33. Wang, X.J.; Wang, X.M.; Hu, X.S.; Wu, K. Effects of hot extrusion on microstructure and mechanical properties of Mg matrix composite reinforced with deformable TC_4 particles. *J. Magnes. Alloy.* **2020**, *8*, 421–430. [CrossRef]

34. Meher, A.; Mahapatra, M.M.; Samal, P.; Vundavilli, P.R. Study on effect of TiB_2 reinforcement on the microstructural and mechanical properties of magnesium RZ5 alloy based metal matrix composites. *J. Magnes. Alloy.* **2020**, *8*, 780–792. [CrossRef]

35. Poddar, P.; Srivastava, V.C.; De, P.K.; Sahoo, K.L. Processing and Mechanical Properties of SiC Reinforced Cast Magnesium Matrix Composites by Stir Casting Process. *Mater. Sci. Eng. A* **2007**, *460–461*, 357–364. [CrossRef]

36. Rauber, C.; Lohmüller, A.; Opel, S.; Singer, R.F. Microstructure and Mechanical Properties of SiC Particle Reinforced Magnesium Composites Processed by Injection Molding. *Mater. Sci. Eng. A* **2011**, *528*, 6313–6323. [CrossRef]

37. Megahed, M.; Attia, M.A.; Abdelhameed, M.; El-Shafei, A.G. Tribological Characterization of Hybrid Metal Matrix Composites Processed by Powder Metallurgy. *Acta Metall. Sin. Engl.* **2017**, *30*, 781–790. [CrossRef]

38. Pu, B.W.; Lin, X.B.; Li, B.W.; Chen, X.F.; He, C.N.; Zhao, N.Q. Effect of SiC Nanoparticles on the Precipitation Behavior and Mechanical Properties of 7075Al Alloy. *J. Mater. Sci.* **2020**, *55*, 6145–6160. [CrossRef]

39. Wang, X.J.; Hu, X.S.; Wu, K.; Wang, L.Y.; Huang, Y.D. Evolutions of Microstructure and Mechanical Properties for SiCp/AZ91 Pomposites with Different Particle Contents during Extrusion. *Mater. Sci. Eng. A* **2015**, *636*, 138–147. [CrossRef]

40. Wang, W.Z.; Chen, X.; Wang, Q.M.; Huang, G.S.; Li, J.B.; Chen, X.H.; Zheng, K.H.; Jiang, B.; Pan, F.S. Microstructural regulation and mechanical behavior of asymmetrically extruded high-content TC$_4$p reinforced AZ31 composite. *Mater. Sci. Eng. A* **2024**, *892*, 146067. [CrossRef]

41. Li, R.G.; Li, H.R.; Zhao, D.Y.; Dai, Y.Q.; Fang, D.Q.; Zhang, J.H.; Zong, L.; Sun, J. High strength commercial AZ91D alloy with a uniformly fine-grained structure processed by conventional extrusion. *Mater. Sci. Eng. A* **2020**, *780*, 139193. [CrossRef]

42. He, Y.J.; Xu, H.Y.; Liu, Y.; Chen, Y.Y.; Ji, Z.S. Strengthening mechanism of B$_4$C@APC/Al matrix composites reinforced with bimodal-sized particles prepared by hydrothermal carbonized deposition on chips. *J. Mater. Sci. Technol.* **2022**, *123*, 60–69. [CrossRef]

43. Sun, X.F.; Wang, C.J.; Deng, K.K.; Kang, J.W.; Bai, Y.; Nie, K.B.; Shang, S.J. Aging Behavior of AZ91 Matrix Influenced by 5 μm SiCp: Investigation on the Microstructure and Mechanical Properties. *J. Alloys Compd.* **2017**, *727*, 1263–1272. [CrossRef]

44. Xu, J.; Jiang, B.; Kang, Y.H.; Zhao, J.; Zhang, W.W.; Zheng, K.H.; Pan, F.S. Tailoring microstructure and texture of Mg–3Al–1Zn alloy sheets through curve extrusion process for achieving low planar anisotropy. *J. Mater. Sci. Technol.* **2022**, *113*, 48–60. [CrossRef]

45. *GB/T228-2002*; Metallic Materials-Tensile Testing at Ambient Temperature. General Administration of Quality Supervision, Inspection and Quarantineof the People's Republic of China: Beijing, China, 2002.

46. Chen, Y.; Yao, Y.; Han, S.L.; Feng, X.W.; Luo, T.G.; Zheng, K.H. Study on Microstructure and Mechanical Properties of TC$_4$/AZ31 Magnesium Matrix Nanocomposites. *Materials* **2023**, *16*, 1139. [CrossRef]

47. Shen, M.J.; Wang, X.J.; Zhang, M.F.; Hu, X.S.; Zheng, M.Y.; Wu, K. Fabrication of Bimodal Size SiCp Reinforced AZ31B Magnesium Matrix Composites. *Mater. Sci. Eng. A* **2014**, *601*, 58–64. [CrossRef]

48. Deng, K.K.; Wang, C.J.; Nie, K.B.; Wang, X.J. Recent Research on the Deformation Behavior of Particle Reinforced Magnesium Matrix Composite: A Review. *Acta Metall. Sin. Engl.* **2019**, *32*, 413–425. [CrossRef]

49. Li, Y.Q.; Li, F.; Kang, F.W.; Du, H.Q.; Chen, Z.Y. Recent research and advances in extrusion forming of magnesium alloys: A review. *J. Alloys Compd.* **2023**, *953*, 170080. [CrossRef]

50. Cui, X.F.; Guo, Y.L.; Yang, Y.; Zhu, Y.; Zhou, G.; Cao, T.T.; Luo, Q.; Wei, G.B.; Li, Q.; Jiang, B.; et al. High-ductility Mg-9Li-1Zn-2Gd-1.2Mn alloy prepared via traditional hot extrusion. *Mater. Sci. Eng. A* **2024**, *893*, 146094. [CrossRef]

51. Lv, S.H.; Xie, Z.F.; Yang, Q.; Meng, F.Z.; Qiu, X. Microstructures and mechanical properties of a hot-extruded Mg–8Zn–6Al–1Gd (wt%) alloy. *J. Alloys Compd.* **2022**, *904*, 164040. [CrossRef]

52. Doherty, R.D.; Hughes, D.A.; Humphreys, F.J.; Jonas, J.J.; Jensen, D.J.; Kassner, M.E.; King, W.E.; McNelley, T.R.; McQueen, H.J.; Rollett, A.D. Current Issues in Recrystallization: A Review. *Mater. Sci. Eng. A* **1997**, *238*, 219–274. [CrossRef]

53. Xu, H.Y.; Yang, Z.; Hu, M.L.; Ji, Z.S. Effect of Short Carbon Fiber Content on SCFs/AZ31 Composite Microstructure and Mechanical Properties. *Results Phys.* **2020**, *17*, 103074. [CrossRef]

54. Wu, K.; Deng, K.K.; Nie, K.B.; Wu, Y.W.; Wang, X.J.; Hu, X.S.; Zheng, M.Y. Microstructure and Mechanical Properties of SiCp/AZ91 Composite Deformed Through a Combination of Forging and Extrusion Process. *Mater. Des.* **2010**, *31*, 3929–3932. [CrossRef]

55. Habibnejad Korayem, M.; Mahmudi, R.; Poole, W.J. Enhanced Properties of Mg-Based Nano-Composites Reinforced with Al$_2$O$_3$ Nano-particles. *Mater. Sci. Eng. A* **2009**, *519*, 198–203. [CrossRef]

56. Chang, H.; Wang, X.J.; Hu, X.S.; Wang, Y.Q.; Nie, K.B.; Wu, K. Effects of Reinforced Particles on Dynamic Recrystallization of Mg Base Alloys during Hot Extrusion. *Rare Met. Mater. Eng.* **2014**, *43*, 1821–1825. [CrossRef]

57. Morisada, Y.; Fujii, H.; Nagaoka, T.; Fukusumi, M. Effect of Friction Stir Processing with SiC Particles on Microstructure and Hardness of AZ31. *Mater. Sci. Eng. A* **2006**, *433*, 50–54. [CrossRef]

58. Shang, S.J.; Deng, K.K.; Nie, K.B.; Li, J.C.; Zhou, S.S.; Xu, F.J.; Fan, J.F. Microstructure and Mechanical Properties of SiCp/Mg–Al–Zn Composites Containing Mg$_{17}$Al$_{12}$ Phases Processed by Low-Speed Extrusion. *Mater. Sci. Eng. A* **2014**, *610*, 243–249. [CrossRef]

59. Alrasheedi, N.H.; Ataya, S.; El-Sayed Seleman, M.M.; Ahmed, M.M.Z. Tensile Deformation and Fracture of Unreinforced AZ91 and Reinforced AZ91-C at Temperatures up to 300 °C. *Materials* **2023**, *16*, 4785. [CrossRef]

60. Luo, H.; Li, J.; Ye, J.; Lu, Y.; Tan, J.; Song, J.; Chen, X.; Zheng, K.; Pan, F. Influence of Ti-6Al-4V particles on the interfacial microstructure and strength-ductility synergetic mechanism of AZ91 magnesium alloy. *Mater. Charact.* **2022**, *191*, 112154. [CrossRef]

61. Rojas, Á.; Sánchez Torrijos, Y.; Gil-Gómez, A.; Liu, C.H.; Rodríguez Rivas, C.; Ferrer, M.T.; Romero Gómez, M. Performance of different biomarkers for the management of hepatocellular carcinoma. *Hepatoma Res.* **2018**, *4*, 31. [CrossRef]

62. Kumar, B.P.; Birru, A.K. Microstructure and mechanical properties of aluminium metal matrix composites with addition of bamboo leaf ash by stir casting method. *Trans. Nonferrous Met. Soc. China* **2017**, *27*, 2555–2572. [CrossRef]

63. Chai, F.; Ma, Z.; Han, X.; Hu, X.; Chang, Z.; Zhou, J. Effect of strain rates on mechanical behavior, microstructure evolution and failure mechanism of extruded-annealed AZ91 magnesium alloy under room-temperature tension. *J. Mater. Res. Technol.* **2023**, *27*, 4644–4656. [CrossRef]

64. Liu, S.S.; Wang, W.Z.; Chen, X.; Huang, G.S.; Liu, H.; Tang, A.; Jiang, B.; Pan, F.S. Enhanced strength and ductility AZ91 alloy with heterogeneous lamella structure prepared by pre-aging and low-temperature extrusion. *Mater. Sci. Eng. A* **2021**, *812*, 141094. [CrossRef]

65. Whelchel, R.L.; Sanders, T.H.; Thadhani, N.N. Spall and dynamic yield behavior of an annealed aluminum–magnesium alloy. *Scr. Mater.* **2014**, *92*, 59–62. [CrossRef]

66. Wang, D.X.; Jing, Y.; Lin, B.S.; Li, J.P.; Shi, Y.; Misra, R.D.K. On the structure, mechanical behavior, and deformation mechanism of AZ91 magnesium alloy processed by symmetric and asymmetric rolling. *Mater. Charact.* **2022**, *194*, 112444. [CrossRef]

67. Deng, K.K.; Wu, K.; Wu, Y.W.; Nie, K.B.; Zheng, M.Y. Effect of Submicron Size SiC Particulates on Microstructure and Mechanical Properties of AZ91 Magnesium Matrix Composites. *J. Alloys Compd.* **2010**, *504*, 542–547. [CrossRef]

68. Fathi, R.; Ma, A.; Saleh, B.; Xu, Q.; Jiang, J.H. Investigation on mechanical properties and wear performance of functionally graded AZ91-SiCp composites via centrifugal casting. *Mater. Today Commun.* **2020**, *24*, 101169. [CrossRef]

69. Raja, A.; Pancholi, V. Effect of friction stir processing on tensile and fracture behaviour of AZ91 alloy. *J. Mater. Process. Technol.* **2017**, *248*, 8–17. [CrossRef]

70. Yuan, Q.H.; Fu, D.M.; Zeng, X.S.; Liu, Y. Fabrication of carbon nanotube reinforced AZ91D composite with superior mechanical properties. *Trans. Nonferrous Met. Soc. China* **2017**, *27*, 1716–1724. [CrossRef]

71. Nai, M.H.; Wei, J.; Gupta, M. Interface tailoring to enhance mechanical properties of carbon nanotube reinforced magnesium composites. *Mater. Des.* **2014**, *60*, 490–495. [CrossRef]

72. Wang, X.J.; Wu, K.; Huang, W.X.; Zhang, H.F.; Zheng, M.Y.; Peng, D.L. Study on fracture behavior of particulate reinforced magnesium matrix composite using in situ SEM. *Compos. Sci. Technol.* **2007**, *67*, 2253–2260. [CrossRef]

73. Huang, S.J.; Abbas, A. Effects of tungsten disulfide on microstructure and mechanical properties of AZ91 magnesium alloy manufactured by stir casting. *J. Alloys Compd.* **2020**, *817*, 153321. [CrossRef]

74. Zhang, Z.; Chen, D.L. Contribution of Orowan Strengthening Effect in Particulate-Reinforced Metal Matrix Nanocomposites. *Mater. Sci. Eng. A* **2008**, *483*, 148–152. [CrossRef]

75. Cubides, Y.; Karayan, A.I.; Vaughan, M.W.; Karaman, I.; Castaneda, H. Enhanced mechanical properties and corrosion resistance of a fine-grained Mg-9Al-1Zn alloy: The role of bimodal grain structure and β-$Mg_{17}Al_{12}$ precipitates. *Materialia* **2020**, *13*, 100840. [CrossRef]

76. Deng, K.K.; Shi, J.Y.; Wang, C.J.; Wang, X.J.; Wu, Y.W.; Nie, K.B. Microstructure and Strengthening Mechanism of Bimodal Size Particle Reinforced Magnesium Matrix Composite. *Compos. Part A* **2012**, *43*, 1280–1284. [CrossRef]